Mechanics of Advanced Composite Structures 12 (2025), Serial Number 26, 585 – 596

Mechanics of Advanced Composite Structures

Journal homepage: https://macs.semnan.ac.ir/

Semnan University

ISSN:2423-7043

Review Article

A New Numerical Solution of 3D Nonlinear Thermo-Mechanical Bending Analysis of Functionally Graded Annular Thick Plate Under Asymmetric Boundary Conditions and Non-Uniform Local Loading

Amir Reza Golkarian [a], Mehrdad Jabbarzadeh [b] *

[a] *Department of Mechanical Engineering, Science & Research Branch, Islamic Azad University, Tehran, Iran*

[b] *Department of Mechanical Engineering, Mashhad Branch, Islamic Azad University, Mashhad, Iran*

ARTICLE INFO

Article history:

Received: 2024-08-11

Revised: 2025-02-12

Accepted: 2025-03-13

Keywords:

Three-dimensional elasticity theory;
Nonlinear,
Asymmetry;
Semi-analytical polynomial method;
functionally graded materials.

ABSTRACT

In this study, the numerical solution of the nonlinear thermo-mechanical bending analysis of functionally graded (FG) annular thick plates, based on 3D elasticity theory and resting on Winkler-Pasternak elastic foundations, is presented under mechanical, thermal, and thermo-mechanical loading using the semi-analytical polynomial method (SAPM). This study represents the first report on the bending analysis of plates under asymmetric boundary conditions and non-uniform local loading. The bending of an FG annular thick plate subjected to general or local, uniform or non-uniform loadings for different symmetric and asymmetric boundary conditions—clamped, simply supported, and free edges—is studied. Considering the fact that no study has been conducted on 3D asymmetric bending analysis, the influences of different positions, areas, intensities, and functions of uniform and non-uniform, general and local loading under symmetric and asymmetric boundary conditions on deflection and thickness variations are investigated and the results are compared with those obtained from ABAQUS software. The most significant result in the case of local loading is one that in some cases, the plate may experience higher deflection than when the general loading covered all areas of the plate.

1. Introduction

Different plate theories have been used to analyze the bending behavior of plates with different shapes, mechanical behaviors, boundary conditions, and types of loading during the last decades. Different plate theories such as classical plate theory (CPT) [1,2], first-order shear deformation theory (FSDT) [2,3], third-order shear deformation theory (TSDT) [4], and higher-order shear deformation theory (HSDT) [5] are used by the literature to investigate the bending behavior of axisymmetric annular/circular plates. However, few studies have examined the bending of annular/circular plates based on 3D elasticity theory such as ones by Yang et al. [6] recently, which investigated the 3D bending of axisymmetric FG graphene-reinforced circular and annular plates.

* **Corresponding author.**
E-mail address: *Jabbarzadeh@mshdiau.ac.ir*

Cite this article as:

Golkarian, A.R. and Jabbarzadeh, M., 2025. A New Numerical Solution of 3D Nonlinear Thermo-Mechanical Bending Analysis of Functionally Graded Annular Thick Plate Under Asymmetric Boundary Conditions and Non-Uniform Local Loading. *Mechanics of Advanced Composite Structures*, 12(3), pp. 586-596.

https://doi.org/10.22075/MACS.2025.34937.1714

Reddy and Berry [7] proposed nonlinear size-dependent models based on Classical Laminate Plate Theory (CLPT) and FSDT for the bending of circular plates. Reddy and Kim [8] utilized MCST and the nonlinear strains of von Karman to develop a size-dependent third-order plate model. Dastjerdi and Jabbarzadeh [9-14] employed Eringen's nonlocal theory and the Differential Quadrature Method (DQM), as well as introduced a new Semi-Analytical Polynomial Method (SAPM), to investigate the nonlinear thermo-mechanical bending of monolayer and bilayer graphene sheets based on FSDT and TSDT. Thai et al. [15–17] proposed new models based on CPT, FSDT, TSDT, and sinusoidal shear deformation plate theories for analyzing the bending and free vibration of rectangular microplates with simply supported edges. Sahmani and Ansari [18] analyzed the free vibration of rectangular microplates using strain gradient theory and TSDT. Using nonlocal elasticity and a Higher-Order Shear Deformation Plate Theory (HSDT), Daneshmehr et al. [19] examined the size-dependent instability of nanoplates under biaxial in-plane loadings, solving the governing equations with the Generalized Differential Quadrature (GDQ) method.

Few studies are devoted to examining the asymmetric bending of plates. For example, Tielking [20] examined the bending of an isotropic annular plate with variable thickness and clamped edges using Von Karman plate theory, the Ritz method, and two-dimensional sinusoidal displacement relations numerically. Pardoen [21] presented a two-dimensional analytical finite element method (FEM) to investigate the bending of a circular plate subjected to a concentrated force. Al Jarbouh Ali [22] developed a mathematical analytical model based on classical plate theory to investigate the behavior of a metallic circular plate under asymmetric loading using Reissner theory.

Also, among the literature, there are some other researchers [23-26] whose review helps to better understand the present study.

To the best of the authors' knowledge, the asymmetric bending analysis of FG (Functionally Graded) annular thick plates under non-uniform local loading and asymmetric boundary conditions has not been investigated or reported in the literature. This gap is due to the lack of numerical or analytical methods capable of solving the bending governing equations of plates under such asymmetric conditions. Therefore, the present study investigates, for the first time, the nonlinear asymmetric bending analysis of FG annular thick plates under asymmetric boundary conditions and uniform and non-uniform, general and local loading based on 3D elasticity theory using the SAPM method, as recently presented by Dastjerdi and Jabbarzadeh [3].SAPM is a powerful semi-analytical polynomial method with significant potential for solving governing equations related to various asymmetry cases in the 3D bending analysis of annular thick plates.

For this purpose, the governing equations of 3D nonlinear bending of FG annular plates are derived using the principle of stationary total potential energy. Then, general or local loadings with different areas, intensities, functions, and positions are applied to the plate under various symmetric and asymmetric boundary conditions. To apply the asymmetric boundary conditions, the plate boundaries are divided into two parts, with different boundary conditions used for each part. The analysis is performed for different types of loading, such as mechanical, thermal, and thermo-mechanical, and the influence of elastic foundations is investigated using Winkler-Pasternak parameters.

2. Governing Equations

2.1. Functionally Graded Materials

FG materials refer to a non-homogeneous category of materials in which the material properties vary gradually and continuously between two points of the solid. These variations can be smooth or sharp, depending on the volume fractions of the constituent materials. Among the most attractive applications of FG materials are wear coating and thermal shielding problems. In this study, a two-constituent functionally graded annular thick plate based on the following formula is employed [2]:

$$\begin{aligned} E(z) &= (E_2 - E_1)\left(\frac{1}{2} + \frac{z}{h}\right)^n + E_1 \\ \alpha(z) &= (\alpha_2 - \alpha_1)\left(\frac{1}{2} + \frac{z}{h}\right)^n + \alpha_1 \end{aligned} \tag{1}$$

where E(z) is the modulus and α(z) is thermal diffusivity, the subscripts 1 and 2 refer to the top and bottom materials, n denotes the volume fraction exponent and h is the plate thickness. A schematic of FG annular thick plate is illustrated in Fig.1 with inner radius r_i, outer radius r_o, the thickness of h under transverse loading q(r,θ) resting on two parameters Winkler-Pasternak elastic foundations, k_w, and kp are the Winkler and Pasternak stiffness coefficients of elastic foundation respectively.

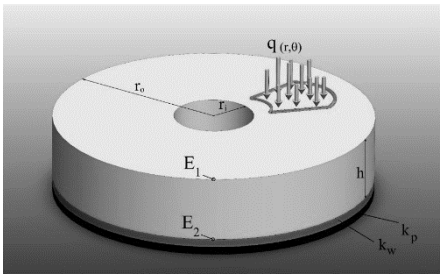

Fig. 1. The schematic view of an FG annular thick plate under non-uniform local loading rested on elastic foundations

2.2. 3D Elasticity Theory Formulation

According to the 3D elasticity theory of plates, the displacement field can be expressed as follows:

$$u_1(r,\theta,z) = u(r,\theta,z) \tag{2}$$

$$u_2(r,\theta,z) = v(r,\theta,z) \tag{3}$$

$$u_3(r,\theta,z) = w(r,\theta,z) \tag{4}$$

where u_i is the displacement vector and u, v, w are the displacement components along the r, θ, z directions respectively. It is evident that no assumptions or simplifications are made in defining the displacement vectors, ensuring that the most accurate results are obtained compared to other theories. The nonlinear components of the Von Karman strain field can be expressed as [27]:

$$\varepsilon_{rr} = \frac{\partial u}{\partial r} + \frac{1}{2}\left(\frac{\partial w}{\partial r}\right)^2 - \alpha(z)\Delta T \tag{5}$$

$$\varepsilon_{\theta\theta} = \frac{u}{r} + \frac{1}{r}\frac{\partial v}{\partial \theta} + \frac{1}{2}\left(\frac{1}{r}\frac{\partial w}{\partial \theta}\right)^2 - \alpha(z)\Delta T \tag{6}$$

$$\varepsilon_{zz} = \frac{\partial w}{\partial z} + \frac{1}{2}\left(\frac{\partial w}{\partial z}\right)^2 - \alpha(z)\Delta T \tag{7}$$

$$\varepsilon_{r\theta} = \frac{1}{2}\left(\frac{1}{r}\frac{\partial u}{\partial \theta} + \frac{\partial v}{\partial r} - \frac{v}{r} + \frac{1}{r}\frac{\partial w}{\partial r}\frac{\partial w}{\partial \theta}\right) \tag{8}$$

$$\varepsilon_{\theta z} = \frac{1}{2}\left(\frac{\partial v}{\partial z} + \frac{1}{r}\frac{\partial w}{\partial \theta} + \frac{1}{r}\frac{\partial w}{\partial \theta}\frac{\partial w}{\partial z}\right) \tag{9}$$

$$\varepsilon_{rz} = \frac{1}{2}\left(\frac{\partial u}{\partial z} + \frac{\partial w}{\partial r} + \frac{\partial w}{\partial r}\frac{\partial w}{\partial z}\right) \tag{10}$$

where ε_{ij} is the stress tensor, δ_{ij} is Kronecker delta symbol, ε_T is thermal strain and ΔT is the temperature difference.

Due to the isotropic behavior of the employed FG plate, the stress-strain relations, according to Hook's Law [2,27], are defined as:

$$\begin{bmatrix}\sigma_{rr}\\ \sigma_{\theta\theta}\\ \sigma_{zz}\\ \sigma_{\theta z}\\ \sigma_{rz}\\ \sigma_{r\theta}\end{bmatrix} = \frac{E(z)}{(1+\upsilon)}\begin{bmatrix}\frac{(1-\upsilon)}{(1-2\upsilon)} & \frac{\upsilon}{(1-2\upsilon)} & \frac{\upsilon}{(1-2\upsilon)} & 0 & 0 & 0\\ \frac{\upsilon}{(1-2\upsilon)} & \frac{(1-\upsilon)}{(1-2\upsilon)} & \frac{\upsilon}{(1-2\upsilon)} & 0 & 0 & 0\\ \frac{\upsilon}{(1-2\upsilon)} & \frac{\upsilon}{(1-2\upsilon)} & \frac{(1-\upsilon)}{(1-2\upsilon)} & 0 & 0 & 0\\ 0 & 0 & 0 & 1 & 0 & 0\\ 0 & 0 & 0 & 0 & 1 & 0\\ 0 & 0 & 0 & 0 & 0 & 1\end{bmatrix}\begin{bmatrix}\varepsilon_{rr}\\ \varepsilon_{\theta\theta}\\ \varepsilon_{zz}\\ \varepsilon_{\theta z}\\ \varepsilon_{rz}\\ \varepsilon_{r\theta}\end{bmatrix} - \begin{bmatrix}\frac{E(z)}{(1-2\upsilon)}\\ \frac{E(z)}{(1-2\upsilon)}\\ \frac{E(z)}{(1-2\upsilon)}\\ 0\\ 0\\ 0\end{bmatrix}\alpha(z)\cdot\Delta T \tag{11}$$

where σ_{ij} is the Cauchy stress, ε_{ij} is the strain and υ is the poison ratio of the FG plate.

2.3. Constitutive Equations

In this study, the constitutive equations and boundary conditions are derived based on the principle of stationary total potential energy [27]:

$$\delta(U - W_{ext}) = 0 \tag{12}$$

where δ is the variation symbol and W_{ext} is the potential of applied forces which contains the effects of transverse loading q(r,θ) and Winkler-Pasternak elastic foundation on the surface of the plate.

The components of total potential energy are defined as:

$$\delta U = \Big(\iiint_V \sigma_{rr}\delta\varepsilon_{rr} + \sigma_{\theta\theta}\delta\varepsilon_{\theta\theta} + \sigma_{zz}\delta\varepsilon_{zz} + \sigma_{rz}\delta\gamma_{rz} + \sigma_{r\theta}\delta\gamma_{r\theta} + \sigma_{\theta z}\delta\gamma_{\theta z}\Big) r\,dr\,d\theta\,dz \tag{13}$$

$$\delta W_{ext} = \int_0^{2\pi}\int_{r_i}^{r_o}\left(q(r,\theta) - k_w w + k_p\nabla^2 w\right)\delta w\,r\,dr\,d\theta \tag{14}$$

where $\nabla^2 = \frac{\partial^2}{\partial r^2} + \frac{1}{r}\frac{\partial}{\partial r} + \frac{1}{r^2}\frac{\partial^2}{\partial \theta^2}$ is the Laplacian operator.

By substituting Eqs. (5)-(10) into the Eq. (13) and neglecting body forces, 3D equilibrium equations of FG annular thick plate are derived as:

$$\delta u = 0 : \frac{\partial \sigma_{rr}}{\partial r} + \frac{1}{r}\frac{\partial \sigma_{r\theta}}{\partial \theta} + \frac{\partial \sigma_{rz}}{\partial z} + \frac{\sigma_{rr} - \sigma_{\theta\theta}}{r} = 0 \qquad (15)$$

$$\delta v = 0 : \frac{\partial \sigma_{r\theta}}{\partial r} + \frac{2}{r}\sigma_{r\theta} + \frac{1}{r}\frac{\partial \sigma_{\theta\theta}}{\partial \theta} + \frac{\partial \sigma_{\theta z}}{\partial z} = 0 \qquad (16)$$

$$\begin{aligned} \delta w = 0 : & \frac{\partial \sigma_{rz}}{\partial r} + \frac{\sigma_{rz}}{r} + \frac{1}{r}\frac{\partial \sigma_{\theta z}}{\partial \theta} + \frac{\partial \sigma_{zz}}{\partial z} + \\ & \frac{1}{r}\frac{\partial}{\partial r}\left(r\sigma_{rr}\frac{\partial w}{\partial r} + \sigma_{r\theta}\frac{\partial w}{\partial \theta} + r\sigma_{rz}\frac{\partial w}{\partial z}\right) + \\ & \frac{1}{r}\frac{\partial}{\partial \theta}\left(\sigma_{r\theta}\frac{\partial w}{\partial r} + \frac{\sigma_{\theta\theta}}{r}\frac{\partial w}{\partial \theta} + \sigma_{\theta z}\frac{\partial w}{\partial z}\right) \\ & + \frac{1}{r}\frac{\partial}{\partial z}\left(r\sigma_{rz}\frac{\partial w}{\partial r} + \sigma_{\theta z}\frac{\partial w}{\partial \theta} + r\sigma_{zz}\frac{\partial w}{\partial z}\right) = 0 \end{aligned} \qquad (17)$$

As the final step, by substituting Eqs. (5)-(10) into Eq. (11) to express the stress components in terms of the displacement fields, and then replacing the resulting stress components into Eqs. (15)-(17), three equilibrium equations are derived as follows:

$$\begin{aligned} \delta u = 0 : & \frac{\partial}{\partial r}\frac{E(z)}{(1+\upsilon)(1-2\upsilon)}\left[(1-\upsilon)\left(\frac{\partial u}{\partial r} + \frac{1}{2}\left(\frac{\partial w}{\partial r}\right)^2\right) + \upsilon\left(\frac{u}{r} + \frac{1}{r}\frac{\partial v}{\partial \theta} + \frac{1}{2}\left(\frac{1}{r}\frac{\partial w}{\partial \theta}\right)^2\right) + \upsilon\left(\frac{\partial w}{\partial z} + \frac{1}{2}\left(\frac{\partial w}{\partial z}\right)^2\right)\right] + \\ & \frac{E(z)}{(1+\upsilon)\cdot r}\frac{\partial}{\partial \theta}\left[\frac{1}{r}\frac{\partial u}{\partial \theta} + \frac{\partial v}{\partial r} - \frac{v}{r} + \frac{1}{r}\frac{\partial w}{\partial r}\frac{\partial w}{\partial \theta}\right] + \frac{\partial}{\partial z}\left(\frac{E(z)}{(1+\upsilon)}\left[\frac{\partial u}{\partial z} + \frac{\partial w}{\partial r} + \frac{\partial w}{\partial r}\frac{\partial w}{\partial z}\right]\right) + \\ & \frac{E(z)(1-\upsilon)}{(1+\upsilon)(1-2\upsilon)}\frac{1}{r}\left(\frac{\partial u}{\partial r} + \frac{1}{2}\left(\frac{\partial w}{\partial r}\right)^2 - \frac{(1+\upsilon)}{\upsilon}\alpha(z)\Delta T\right) + \frac{\upsilon\cdot E(z)}{(1+\upsilon)(1-2\upsilon)}\frac{1}{r} \\ & \left(\frac{u}{r} + \frac{1}{r}\frac{\partial v}{\partial \theta} + \frac{1}{2}\left(\frac{1}{r}\frac{\partial w}{\partial \theta}\right)^2 - \frac{(1+\upsilon)}{\upsilon}\alpha(z)\Delta T\right) + \frac{\upsilon\cdot E(z)}{(1+\upsilon)(1-2\upsilon)}\frac{1}{r}\left(\frac{\partial w}{\partial z} + \frac{1}{2}\left(\frac{\partial w}{\partial z}\right)^2 - \frac{(1+\upsilon)}{\upsilon}\alpha(z)\Delta T\right) - \\ & \frac{1}{r}\left(\frac{E(z)}{(1-2\upsilon)}\right)\alpha(z)\Delta T - \frac{E(z)(1-\upsilon)}{(1+\upsilon)(1-2\upsilon)}\frac{1}{r}\left(\frac{\partial u}{\partial r} + \frac{1}{2}\left(\frac{\partial w}{\partial r}\right)^2 - \alpha(z)\Delta T\right) - \\ & \frac{\upsilon\cdot E(z)}{(1+\upsilon)(1-2\upsilon)}\frac{1}{r}\left(\frac{u}{r} + \frac{1}{r}\frac{\partial v}{\partial \theta} + \frac{1}{2}\left(\frac{1}{r}\frac{\partial w}{\partial \theta}\right)^2 - \alpha(z)\Delta T\right) - \\ & \frac{\upsilon\cdot E(z)}{(1+\upsilon)(1-2\upsilon)}\frac{1}{r}\left(\frac{\partial w}{\partial z} + \frac{1}{2}\left(\frac{\partial w}{\partial z}\right)^2 - \alpha(z)\Delta T\right) + \frac{1}{r}\left(\frac{E(z)}{(1-2\upsilon)}\right)\alpha(z)\Delta T = 0 \end{aligned} \qquad (18)$$

$$\begin{aligned} \delta v = 0 : & \frac{E(z)}{(1-2\upsilon)}\frac{\partial}{\partial r}\left[\frac{1}{r}\frac{\partial u}{\partial \theta} + \frac{\partial v}{\partial r} - \frac{v}{r} + \frac{1}{r}\frac{\partial w}{\partial r}\frac{\partial w}{\partial \theta}\right] + \frac{E(z)}{(1-2\upsilon)}\frac{2}{r}\left[\frac{1}{r}\frac{\partial u}{\partial \theta} + \frac{\partial v}{\partial r} - \frac{v}{r} + \frac{1}{r}\frac{\partial w}{\partial r}\frac{\partial w}{\partial \theta}\right] + \\ & \frac{1}{r}\frac{\partial}{\partial \theta}\left[\begin{array}{l} \frac{E(z)(1-\upsilon)}{(1+\upsilon)(1-2\upsilon)}\left(\frac{\partial u}{\partial r} + \frac{1}{2}\left(\frac{\partial w}{\partial r}\right)^2\right) + \frac{\upsilon\cdot E(z)}{(1+\upsilon)(1-2\upsilon)}\left(\frac{u}{r} + \frac{1}{r}\frac{\partial v}{\partial \theta} + \frac{1}{2}\left(\frac{1}{r}\frac{\partial w}{\partial \theta}\right)^2\right) + \\ \frac{\upsilon\cdot E(z)}{(1+\upsilon)(1-2\upsilon)}\left(\frac{\partial w}{\partial z} + \frac{1}{2}\left(\frac{\partial w}{\partial z}\right)^2\right) \end{array}\right] + \\ & \frac{E(z)}{(1-2\upsilon)}\frac{\partial}{\partial z}\left(\frac{\partial v}{\partial z} + \frac{1}{r}\frac{\partial w}{\partial \theta} + \frac{1}{r}\frac{\partial w}{\partial \theta}\frac{\partial w}{\partial z}\right) = 0 \end{aligned} \qquad (19)$$

$$\delta w = 0: \frac{E(z)}{(1-2\upsilon)}\frac{\partial}{\partial r}\left(\frac{\partial u}{\partial z}+\frac{\partial w}{\partial r}+\frac{\partial w}{\partial r}\frac{\partial w}{\partial z}\right)+\frac{E(z)}{(1-2\upsilon)r}\frac{\partial}{\partial r}\left(\frac{\partial u}{\partial z}+\frac{\partial w}{\partial r}+\frac{\partial w}{\partial r}\frac{\partial w}{\partial z}\right)+$$

$$\frac{E(z)}{(1-2\upsilon)r}\frac{\partial}{\partial \theta}\left(\frac{\partial v}{\partial z}+\frac{1}{r}\frac{\partial w}{\partial \theta}+\frac{1}{r}\frac{\partial w}{\partial \theta}\frac{\partial w}{\partial z}\right)+$$

$$\frac{\partial}{\partial z}\left[\begin{array}{l}\frac{(1-\upsilon)\cdot E(z)}{(1+\upsilon)(1-2\upsilon)}\left(\frac{\partial u}{\partial r}+\frac{1}{2}\left(\frac{\partial w}{\partial r}\right)^2\right)+\frac{\upsilon\cdot E(z)}{(1+\upsilon)(1-2\upsilon)}\left(\frac{u}{r}+\frac{1}{r}\frac{\partial v}{\partial \theta}+\frac{1}{2}\left(\frac{1}{r}\frac{\partial w}{\partial \theta}\right)^2\right)+\\ \frac{\upsilon\cdot E(z)}{(1+\upsilon)(1-2\upsilon)}\left(\frac{\partial w}{\partial z}+\frac{1}{2}\left(\frac{\partial w}{\partial z}\right)^2\right)-\frac{E(z)}{(1-2\upsilon)}\alpha\Delta T\end{array}\right]$$

$$+\frac{\partial}{\partial r}\left[\left(\begin{array}{l}\frac{(1-\upsilon)\cdot E(z)}{(1+\upsilon)(1-2\upsilon)}\left(\frac{\partial u}{\partial r}+\frac{1}{2}\left(\frac{\partial w}{\partial r}\right)^2\right)+\frac{\upsilon\cdot E(z)}{(1+\upsilon)(1-2\upsilon)}\left(\frac{u}{r}+\frac{1}{r}\frac{\partial v}{\partial \theta}+\frac{1}{2}\left(\frac{1}{r}\frac{\partial w}{\partial \theta}\right)^2\right)+\\ \frac{\upsilon\cdot E(z)}{(1+\upsilon)(1-2\upsilon)}\left(\frac{\partial w}{\partial z}+\frac{1}{2}\left(\frac{\partial w}{\partial z}\right)^2\right)\end{array}\right)r\frac{\partial w}{\partial r}\right]$$

$$+\frac{E(z)}{(1-2\upsilon)}\frac{\partial}{\partial r}\left[\left(\frac{1}{r}\frac{\partial u}{\partial \theta}+\frac{\partial v}{\partial r}-\frac{v}{r}+\frac{1}{r}\frac{\partial w}{\partial r}\frac{\partial w}{\partial \theta}\right)\frac{\partial w}{\partial \theta}\right]+\frac{E(z)}{(1-2\upsilon)}\frac{\partial}{\partial r}\left[\left(\frac{\partial u}{\partial z}+\frac{\partial w}{\partial r}+\frac{\partial w}{\partial r}\frac{\partial w}{\partial z}\right)\cdot r\frac{\partial w}{\partial z}\right]+$$

$$\frac{E(z)}{(1-2\upsilon)}\frac{\partial}{\partial \theta}\left[\left(\frac{1}{r}\frac{\partial u}{\partial \theta}+\frac{\partial v}{\partial r}-\frac{v}{r}+\frac{1}{r}\frac{\partial w}{\partial r}\frac{\partial w}{\partial \theta}\right)\frac{\partial w}{\partial r}\right]+\frac{E(z)}{(1-2\upsilon)}\frac{\partial}{\partial \theta}\left[\left(\frac{\partial v}{\partial z}+\frac{1}{r}\frac{\partial w}{\partial \theta}+\frac{1}{r}\frac{\partial w}{\partial \theta}\frac{\partial w}{\partial z}\right)\frac{\partial w}{\partial z}\right]+ \quad (20)$$

$$\frac{1}{r}\frac{\partial}{\partial \theta}\left[\left(\begin{array}{l}\frac{(1-\upsilon)E(z)}{(1+\upsilon)(1-2\upsilon)}\left(\frac{\partial u}{\partial r}+\frac{1}{2}\left(\frac{\partial w}{\partial r}\right)^2\right)+\frac{\upsilon\cdot E(z)}{(1+\upsilon)(1-2\upsilon)}\left(\frac{u}{r}+\frac{1}{r}\frac{\partial v}{\partial \theta}+\frac{1}{2}\left(\frac{1}{r}\frac{\partial w}{\partial \theta}\right)^2\right)\\ +\frac{\upsilon\cdot E(z)}{(1+\upsilon)(1-2\upsilon)}\left(\frac{\partial w}{\partial z}+\frac{1}{2}\left(\frac{\partial w}{\partial z}\right)^2\right)\end{array}\right)\frac{\partial w}{\partial \theta}\right]$$

$$+\frac{E(z)}{(1-2\upsilon)}\frac{\partial}{\partial z}\left[\left(\frac{\partial u}{\partial z}+\frac{\partial w}{\partial r}+\frac{\partial w}{\partial r}\frac{\partial w}{\partial z}\right)\cdot r\frac{\partial w}{\partial r}\right]+\frac{\partial}{\partial z}\left[\frac{E(z)}{(1-2\upsilon)}\left(\frac{\partial v}{\partial z}+\frac{1}{r}\frac{\partial w}{\partial \theta}+\frac{1}{r}\frac{\partial w}{\partial \theta}\frac{\partial w}{\partial z}\right)\frac{\partial w}{\partial \theta}\right]+$$

$$\frac{\partial}{\partial z}\left[\left(\begin{array}{l}\frac{(1-\upsilon)\cdot E(z)}{(1+\upsilon)(1-2\upsilon)}\left(\frac{\partial u}{\partial r}+\frac{1}{2}\left(\frac{\partial w}{\partial r}\right)^2\right)+\frac{\upsilon\cdot E(z)}{(1+\upsilon)(1-2\upsilon)}\left(\frac{u}{r}+\frac{1}{r}\frac{\partial v}{\partial \theta}+\frac{1}{2}\left(\frac{1}{r}\frac{\partial w}{\partial \theta}\right)^2\right)+\\ \frac{\upsilon\cdot E(z)}{(1+\upsilon)(1-2\upsilon)}\left(\frac{\partial w}{\partial z}+\frac{1}{2}\left(\frac{\partial w}{\partial z}\right)^2\right)\end{array}\right)\cdot r\frac{\partial w}{\partial z}\right]=0$$

3. Solution Procedure

Given the three equilibrium equations, a system of nonlinear partial differential equations is obtained. In the present study, a new semi-analytical polynomial method (SAPM), recently introduced by Dastjerdi and Jabbarzadeh [3], is employed. This method can solve the system of nonlinear partial differential equations without requiring any assumptions or simplifications.

Using this method, each function in the partial differential equations is approximated by a polynomial in general form, dependent on the distribution of grid points. Unlike traditional solution methods, each polynomial does not need to satisfy boundary conditions explicitly. This approach allows for the convenient and rapid solution of each partial equation or set of equations, accommodating various types of boundary and surface conditions. By considering a partial differential equation as follows:

$$\frac{\partial^n F(r,\theta,z)}{\partial^n r}+\frac{\partial^{(n-1)} F(r,\theta,z)}{\partial^{(n-1)} r}+\cdots+\frac{\partial F(r,\theta,z)}{\partial r}+\frac{\partial^n F(r,\theta,z)}{\partial^n z}+\frac{\partial^{(n-1)} F(r,\theta,z)}{\partial^{(n-1)} z}+\cdots+\frac{\partial F(r,\theta,z)}{\partial z}+\frac{\partial^n F(r,\theta,z)}{\partial^n \theta}+$$
$$\frac{\partial^{(n-1)} F(r,\theta,z)}{\partial^{(n-1)} \theta}+\cdots+\frac{\partial F(r,\theta,z)}{\partial \theta}+\frac{\partial^n F(r,z)}{\partial r \partial^{(n-1)} z}+\frac{\partial^n F(r,z)}{\partial^2 r \partial^{(n-2)} z}+\cdots+\frac{\partial^n F(r,z)}{\partial r^{(n-1)} \partial z}+\frac{\partial^n F(r,z)}{\partial r \partial^{(n-1)} \theta}+\frac{\partial^n F(r,z)}{\partial^2 r \partial^{(n-2)} \theta}+\cdots+$$
$$\frac{\partial^n F(r,z)}{\partial r^{(n-1)} \partial \theta}+\frac{\partial^n F(r,z)}{\partial \theta \partial^{(n-1)} z}+\frac{\partial^n F(r,z)}{\partial^2 \theta \partial^{(n-2)} z}+\cdots+\frac{\partial^n F(r,z)}{\partial \theta^{(n-1)} \partial z}+\frac{\partial^n F(r,z)}{\partial r \partial^{(n-1)} z}+\frac{\partial^n F(r,z)}{\partial r \partial \theta \partial^{(n-2)} z}+\frac{\partial^n F(r,z)}{\partial^2 r \partial \theta \partial^{(n-3)} z}+ \quad (21)$$
$$\frac{\partial^n F(r,z)}{\partial^2 r \partial^2 \theta \partial^{(n-4)} z}+\cdots+\frac{\partial^n F(r,z)}{\partial^{(n-2)} r \partial^{(n-2)} \theta \partial^4 z}+\frac{\partial^n F(r,z)}{\partial^{(n-1)} r \partial^{(n-2)} \theta \partial^3 z}+\frac{\partial^n F(r,z)}{\partial^{(n-1)} r \partial^{(n-1)} \theta \partial^2 z}+\frac{\partial^n F(r,z)}{\partial^{(n-1)} r \partial z}=0$$

where the function $F(r,\theta,z)$ is defined as:

$$F(r,\theta,z)=\sum_{i=1}^{N}\sum_{j=1}^{M}\sum_{k=1}^{P} a_l r^{(i-1)}\theta^{(j-1)} z^{(k-1)} \quad (22)$$

where N is the number of grid points in the r direction, M is the number of grid points in θ direction and P is the number of grid points in the z direction, and l is counted from 1 to $N\times M\times P$ by counting i, j, k on the summations, which sample grid point domains are shown in Fig. 2.

By substituting Eq. (22) in Eq. (21) the partial differential equation is converted to the algebraic equations which $2M\times P$ number of equations would be derived from surface and boundary conditions (black points) and $(N\times M\times P)-(2M\times P)$ number of equations are derived from Eq. (22) (related to the white points). Consequently, there are $N\times M\times P$ numbers of algebraic equations and unknown a_i coefficients which by substituting obtained a_i into the Eq. (22) the function $F(r,\theta,z)$ would be determined. For a system of partial differential equations, similar procedures should be applied.

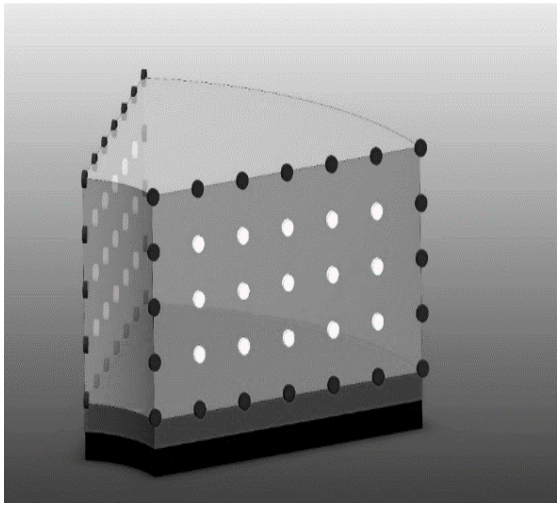

Fig. 2. The schematic view of grid points based on SAPM

Due to the above explanations about SAPM, three displacement fields could be defined as follows:

$$u(r,\theta,z)=\sum_{i=1}^{N}\sum_{j=1}^{M}\sum_{k=1}^{P} a_l r^{(i-1)}\theta^{(j-1)} z^{(k-1)} \quad (23)$$

$$v(r,\theta,z)=\sum_{i=1}^{N}\sum_{j=1}^{M}\sum_{k=1}^{P} a_{l+MNP} r^{(i-1)}\theta^{(j-1)} z^{(k-1)} \quad (24)$$

$$w(r,\theta,z)=\sum_{i=1}^{N}\sum_{j=1}^{M}\sum_{k=1}^{P} a_{l+2MNP} r^{(i-1)}\theta^{(j-1)} z^{(k-1)} \quad (25)$$

The obtained algebraic equations are solved using numerical methods, such as the Newton-Raphson method.

4. Boundary Conditions

In this study, all types of boundary conditions are categorized into three types: simply supported (S), clamped (C), and free edges (F). At the inner and outer radius (ri and ro) the boundary conditions can be defined as follows:

$$S: \sigma_r = v = w = 0 \quad (26)$$

$$C: u = v = w = 0 \quad (27)$$

$$F: \sigma_r = \sigma_{r\theta} = \sigma_{rz} + \sigma_r \frac{\partial w}{\partial r} + \frac{1}{r}\sigma_{r\theta}\frac{\partial w}{\partial \theta} + \sigma_{rz}\frac{\partial w}{\partial z} = 0 \quad (28)$$

In the present study, to define asymmetric boundary conditions, the plate's grid points along the radial direction are divided into two parts (See Fig. 3). Each part must satisfy specific boundary conditions, a possibility made feasible by the use of SAPM. As previously mentioned, this method does not require each polynomial to satisfy boundary conditions explicitly, allowing each partial equation or set of equations to be solved while accommodating various boundary conditions.

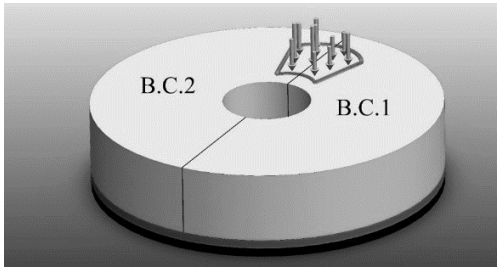

Fig. 3. The schematic view of an annular plate with asymmetric boundary conditions (two parts B.Cs.)

Also, the displacement components should satisfy the following boundary conditions at the top and bottom surfaces of the plate:

$$\sigma_{rz}\big|_{z=-\frac{h}{2},\frac{h}{2}}=0 \tag{29}$$

$$\sigma_{\theta z}\big|_{z=-\frac{h}{2},\frac{h}{2}}=0 \tag{30}$$

$$\sigma_{zz}+\sigma_{zz}\frac{\partial w}{\partial z}+\sigma_{rz}\frac{\partial w}{\partial r}+\frac{1}{r}\sigma_{\theta z}\frac{\partial w}{\partial \theta}\Big|_{z=-\frac{h}{2}}=0 \tag{31}$$

$$\sigma_{zz}+\sigma_{zz}\frac{\partial w}{\partial z}+\sigma_{rz}\frac{\partial w}{\partial r}+\frac{1}{r}\sigma_{\theta z}\frac{\partial w}{\partial \theta}\Big|_{z=-\frac{h}{2}}=0 \tag{32}$$
$$-q(r,\theta)$$

$$\sigma_{zz}+\sigma_{zz}\frac{\partial w}{\partial z}+\sigma_{rz}\frac{\partial w}{\partial r}+\frac{1}{r}\sigma_{\theta z}\frac{\partial w}{\partial \theta}+\Big|_{z=\frac{h}{2}}=0 \tag{33}$$
$$k_w w-k_p\left(\frac{\partial^2 w}{\partial r^2}+\frac{1}{r}\frac{\partial w}{\partial r}\right)$$

In the present study, due to the application of local non-uniform loading, the term is used for the top surface conditions. Additionally, Eqs. (29)-(31) are defined for the grid points at the top surface that are not subjected to local loading, while Eqs. (29), (30), and (32) are used for the grid points under local loading. Eqs. (29), (30), and (33) are defined for the bottom surface grid points.

5. Numerical Results and Discussions

To investigate the convergence of the SAPM, various grid sizes are considered for an FG annular thick plate with the properties listed in [2] (no specific units are used) under symmetric uniform loading. Different boundary conditions are employed, and the results for maximum deflection are reported in Table 1.

$$E_1=10^6; E_2=10^5; \upsilon=0.25; r_o=1; r_i=0.25; \quad h=0.2; q(r,\theta)=50; n=1 \tag{34}$$

which the number of grid points is defined as $n\times m\times p$ which are through r, θ, and z directions. It is observed that the convergence at 9 grid points through the r direction occurred. For all cases, the number of grid points through θ and z directions is 5 points, and for less amount of grid numbers, no exact results are observed for upper grid numbers no considerable change is observed. Also, to examine the accuracy of the results, the FEM results using ABAQUS software are compared with the presented results at the convergence point in Table 1 which good agreement is observed.

To validate the present model and solution procedure, and to compare the results obtained using the present 3D elasticity theory with other theories such as First Order Shear Deformation Theory (FSDT), Third Order Shear Deformation Theory (TSDT), and Fourth Order Shear Deformation Theory (FOSDT), the maximum non-dimensional symmetric deflections of a circular thick plate are compared. The comparison, based on the following non-dimensional properties and clamped boundary conditions for various volume fraction exponents, is presented in Table 2.

$$E_1/E_2=0.396; \upsilon=0.288; h/r_o=0.2; \quad q/E_2=0.05 \tag{35}$$

which good agreement is observed.

In continue, to study the asymmetric bending, an FG thick annular plate with the following properties is employed [2]:

Table 1. Convergence checking of maximum symmetric deflection of an FG annular thick plate versus the number of grid points for various boundary conditions and comparing with FEM results

N. (number of domain nodes)	w					
	Boundary Condition Type					
	C - C	S - S	C - S	S - C	F - C	F - S
7 × 5 × 5	0.000249	0.000774	0.000481	0.000360	0.002797	0.01543
9 × 5 × 5	0.000252	0.000775	0.000480	0.000362	0.002481	0.01440
11 × 5 × 5	0.000253	0.000775	0.000480	0.000361	0.002441	0.01448
FEM	0.000253	0.000782	0.000479	0.000370	0.002525	0.01377

Table 2. Comparison of the maximum non-dimensional symmetric deflection of an FG circular thick plate with clamped edge and various volume fraction exponent by different theories

Study	w*				
	n = 0	n = 2	n = 4	n = 5	n = 6
FSDT [28]	2.979	1.613	1.473	-	1.404
FSDT [29]	2.979	1.613	-	1.434	-
TSDT [29]	2.968	1.603	-	1.423	-
FOSDT [29]	2.968	1.603	-	1.423	-
3D elasticity [Present study]	3.037	1.691	1.474	1.422	1.407

$$E_1 = 10^6; E_2 = 10^5; \upsilon = 0.25; \alpha_1 = 2.2\times10^{-5}; \quad \alpha_2 = 1.5\times10^{-5}; r_o = 1; r_i = 0.25; h = 0.2; n = 1 \tag{36}$$

To investigate the influence of non-uniform loading, four types of general non-uniform transverse loading with symmetric clamped inner and outer edges are employed:

a) linear loading as
$q(r,\theta) = 50\cdot(r-r_o)\cdot(r-r_i)\cdot(\theta)\cdot(\theta-2\pi)$,

b) sinusoidal loading as
$q(r,\theta) = 50\cdot \mathrm{Sin}(r-r_o)\cdot \mathrm{Sin}(r-r_i)\cdot \mathrm{Sin}(\theta/2)$,

c) logarithm loading as
$q(r,\theta) = 50\cdot \log10(r/r_o)\cdot \log10(r/r_i)\cdot \mathrm{Sin}(\theta/2)$
and

d) exponential loading as
$q(r,\theta) = 50\cdot e^{(r-r_o)}\cdot e^{(r-r_i)}\cdot \mathrm{Sin}(\theta/2)$

which the results are reported in Table 3.

Due to no study reporting the bending of the thick annular plate under non-uniform loading, the same FE model is created in ABAQUS software and the results are compared. The results are in good agreement which this point validates the potential of the presented method in bending analysis under non-uniform loading.

To examine and validate the effect of asymmetric boundary conditions, the plate is divided into two parts. The first boundary condition, referred to as B.C. 1, is applied to one part, while the second boundary condition, referred to as B.C. 2, is applied to the other part. The influence of different combinations of boundary conditions on the inner and outer edges under uniform loading as $q(r,\theta) = 50$ is examined. The results, compared with FEM results, are reported in Table 4. The findings indicate a good agreement between the results.

Table 3. The comparison of the maximum deflection of FG annular thick plate under uniform loading with different asymmetric boundary conditions

B.C. 1	B.C. 2	w	
		FEM	Present study
C – C	S – S	0.00070	0.00080
C – S	S – C	0.00046	0.00048
C – C	F – F	0.0380	0.0370
S – S	F – F	0.0380	0.0370

In this part, the influence of uniform local loading on the bending of FG thick plate for two types of symmetric boundary conditions: clamped and simply-supported edges is studied. The study is performed under two categories of transverse loading.

Initially a uniform local loading (Fig. 4) as $q(r,\theta) = 50$ is used in which the load covers a half part of the r direction (middle part) and extends through the direction step by step (type 1). In the first step, the load is distributed through $\pi/2$ rad of θ direction and at each step of analysis is extended by $\pi/2$ rad till it covers all areas of the plate. The results related to this part of the study are illustrated in Fig. 5. To validate the results, the same FEM using ABAQUS software is produced and the results are compared. From the results, it can be deduced that the presented model can simulate the bending behavior of such an FG thick plate under local loading as well.

Table 4. The comparison of the maximum deflection of FG annular thick plate under non-uniform loading with clamped inner and outer edges

Loading	*w*	
	Present study	FEM
$q(r,\theta) = 50\cdot(r-r_o)\cdot(r-r_i)\cdot(\theta)\cdot(\theta-2\pi)$	0.000291	0.000261
$q(r,\theta) = 50\cdot \mathrm{Sin}(r-r_o)\cdot \mathrm{Sin}(r-r_i)\cdot \mathrm{Sin}(\theta/2)$	0.0000278	0.0000278
$q(r,\theta) = 50\cdot \log10(r/r_o)\cdot \log10(r/r_i)\cdot \mathrm{Sin}(\theta/2)$	0.0000177	0.0000157
$q(r,\theta) = 50\cdot(e^{(r-r_o)}-1)\cdot(e^{(r-r_i)}-1)\cdot \mathrm{Sin}(\theta/2)$	0.000030	0.000028

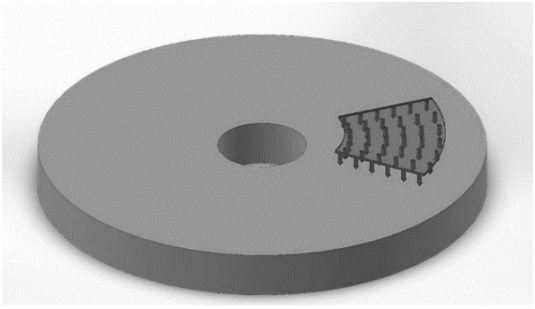

Fig. 4. The schematic view of an annular plate under uniform local loading (type 1)

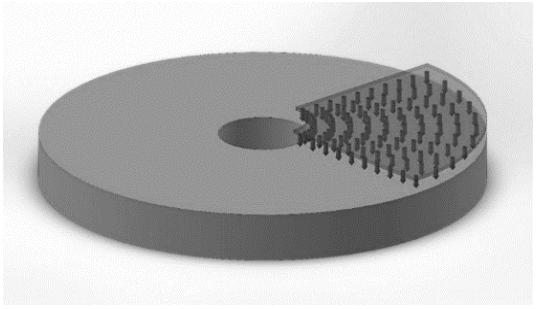

Fig. 6. The schematic view of an annular plate under uniform local loading (type 2)

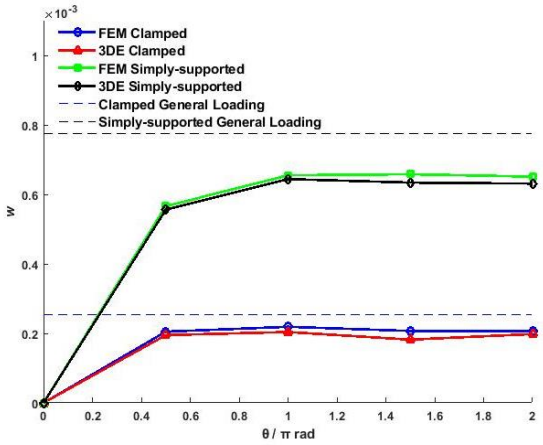

Fig. 5. The variation and comparison of maximum deflection of an annular plate under local loading (type1) for symmetric boundary conditions

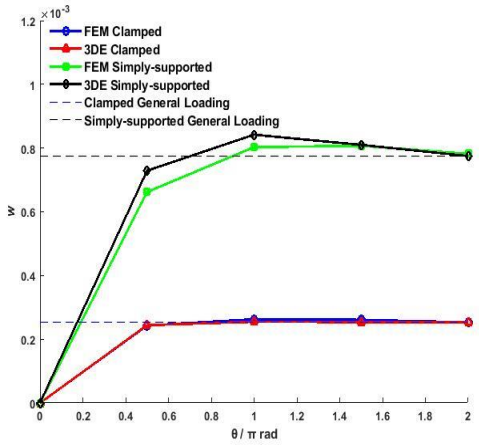

Fig. 7. The variation and comparison of maximum deflection of an annular plate under local loading (type2) for symmetric boundary conditions

In the second part of using uniform local loading, loading as Fig. 6 is used with the same intensity ($q(r,\theta)=50$) but the load is distributed through the r direction completely and extended through θ direction step by step (type 2).

The results related to this part of the study are illustrated in Fig. 7 and compared with FEM results. The results indicate that the plate may experience higher deflection under local loading compared to a plate subjected to general loading with the same intensity. This effect is more pronounced in plates with simply supported edges. Conversely, when local loading is applied to a plate with clamped edges, the deflection initially reaches the maximum deflection observed under general loading. Extending the local loading does not result in significant changes in the maximum deflection of the plate. These observations were not considered in the previous case, where deflection under local loading type 1 was less than under general loading.

To report the maximum deflection under non-uniform local loading and asymmetric boundary conditions, the local loading type 2 with the area of $\pi/2$ rad of θ direction and four different functions is applied to an annular plate with two parts boundary conditions (one C-C and another S-S part) which the load is divided between two parts. Half of the loading area is distributed through the part with a clamped edge and half of that is distributed through the part with a simply-supported edge. Employed loading functions are:

a) linear loading as
$q(r,\theta)=50\cdot(r-r_o)\cdot(r-r_i)\cdot(\theta)\cdot(\theta-2\pi)$,

b) sinusoidal loading as
$q(r,\theta)=50\cdot\mathrm{Sin}(r-r_o)\cdot\mathrm{Sin}(r-r_i)\cdot\mathrm{Sin}(\theta/2)$,

c) logarithm loading as
$q(r,\theta)=50\cdot\log10(r/r_o)\cdot\log10(r/r_i)\cdot\mathrm{Sin}(\theta/2)$

and

d) exponential loading as
$q(r,\theta)=50\cdot e^{(r-r_o)}\cdot e^{(r-r_i)}\cdot\mathrm{Sin}(\theta/2)$.

Table 5. The comparison of the maximum deflection of FG annular thick plate under non-uniform local loading (type 1 of local loading) with two parts (C-C & S-S) boundary conditions

Loading	w			
	Present study		FEM	
	Clamped part	Simply-support part	Clamped part	Simply-support part
$q(r,\theta)=50\cdot(r-r_o)\cdot(r-r_i)\cdot(\theta)\cdot(\theta-2\pi)$	0.000044	0.000077	0.000044	0.000079
$q(r,\theta)=50\cdot\mathrm{Sin}(r-r_o)\cdot\mathrm{Sin}(r-r_i)\cdot\mathrm{Sin}(\theta/2)$	0.0000035	0.0000063	0.0000030	0.0000065
$q(r,\theta)=50\cdot\log10(r/r_o)\cdot\log10(r/r_i)\cdot\mathrm{Sin}(\theta/2)$	0.0000018	0.0000037	0.0000018	0.0000039
$q(r,\theta)=50\cdot(e^{(r-r_o)}-1)\cdot(e^{(r-r_i)}-1)\cdot\mathrm{Sin}(\theta/2)$	0.0000034	0.0000068	0.0000033	0.0000071

The maximum deflection of each part is reported separately and compared in Table 5. The results are in good agreement.

Some discrepancies could be observed during some table outcomes and the most important reason is due to the fact that the way of defining boundary conditions in analytical methods is different than those by FEM. Especially, when the percent of simply-supported boundary conditions is increased, these discrepancies arise which is due to the differences in defining of degree of freedom in the two mentioned methods. It is observed, that by employing fully clamped boundary conditions, the results are in the best agreement.

In continue, the effect of elastic parameters variations on the maximum deflection of the plate under $q(r,\theta)=50\cdot\mathrm{Sin}(r-r_o)\cdot\mathrm{Sin}(r-r_i)\cdot\mathrm{Sin}(\theta/2)$ and two parts of boundary conditions (one C-C and another S-S part) are investigated. Initially, $k_w=10^5$ is used and the effect of Pasternak parameter variation is investigated the result is illustrated in Fig. 8 and then $k_p=10^4$ is used and the effect of Winkler parameter variation is examined (Fig. 9). It is considered that by increasing the elastic parameters the boundary conditions effect is omitted and the deflections of both parts are converged to the same point.

In the last part, the influence of thermo-mechanical loading is investigated for the same plate with non-uniform local loading and asymmetric boundary conditions when the elastic foundation parameters are $k_w=10^5, k_p=10^2$. The variation of deflection and thickness of the plate are illustrated in Figs. 10 and 11. It is considered that by increasing the temperature, the deflection and thickness variation are increased linearly.

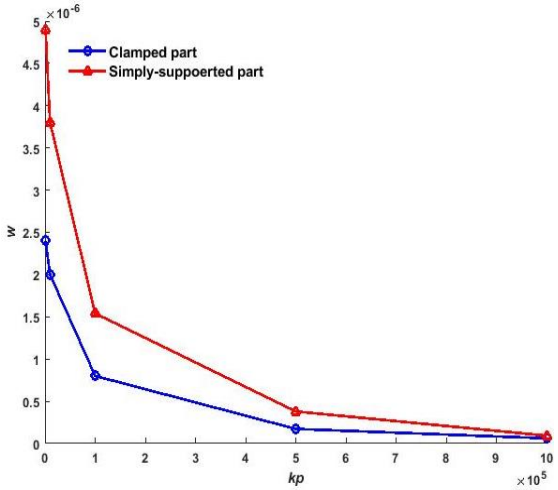

Fig. 8. The variation of maximum deflection of FG annular thick plate under non-uniform local loading with two parts S-S & C-C boundary conditions versus Pasternak foundation parameter variations

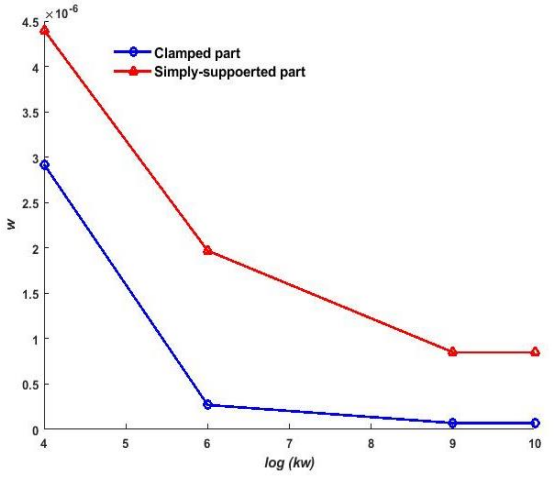

Fig. 9. The variation of maximum deflection of FG annular thick plate under non-uniform local loading with two parts S-S & C-C boundary conditions versus Winkler foundation parameter variations

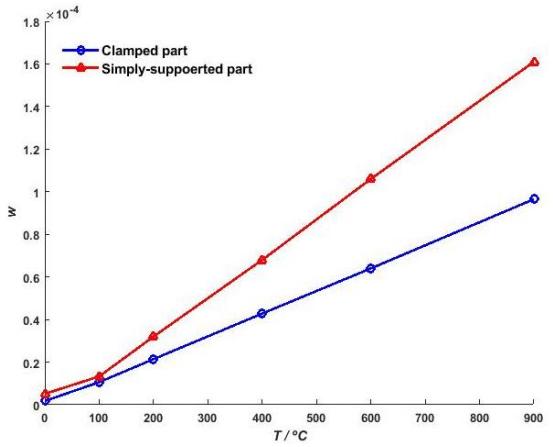

Fig. 10. The variation of maximum deflection of FG annular thick plate under non-uniform local loading with two parts S-S & C-C boundary conditions versus thermal variations

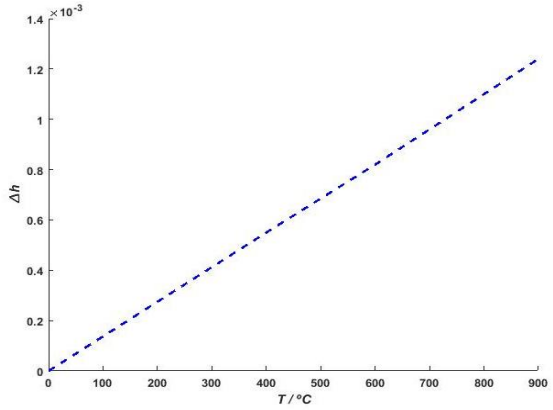

Fig. 11. The variation of thickness of FG annular thick plate under non-uniform local loading with two parts S-S & C-C boundary conditions versus thermal variations

6. Conclusions

In this study, the nonlinear thermo-mechanical bending analysis of an FG thick annular plate under uniform and non-uniform, general and local loading, as well as symmetric and asymmetric boundary conditions, is investigated based on 3D elasticity theory using the SAPM.

The plate is supported on Winkler-Pasternak elastic foundations, and various types of loading—thermal, mechanical, and thermo-mechanical—are applied.

Since no previous studies have reported such an asymmetric bending analysis, a finite element model using ABAQUS software was created to validate the obtained results.

Following comparisons have been done during the study and good agreement is observed:

- The results obtained from different plate theories such as FSDT, TSDT, and FOSDT are compared with those resulting from 3D elasticity theory.
- The results under different non-uniform transverse loading and various asymmetric boundary conditions are compared.
- The influence of various types of uniform and non-uniform local loading under different boundary conditions is examined.
- Both deflection and thickness variations are studied under thermal variations.

In all cases, the results show good agreement with those from FEM, demonstrating the acceptability of the presented method.

The most significant result in the case of local loading is that, in some instances, the plate may experience higher deflection compared to when general loading covers the entire area of the plate.

The study reports the impact of thermo-mechanical non-uniform local loading under asymmetric boundary conditions with elastic foundations on both the deflection and thickness variation of the plate.

Funding Statement

This research did not receive any specific grant from funding agencies in the public, commercial, or not-for-profit sectors.

Conflicts of Interest

The author declares that there is no conflict of interest regarding the publication of this article.

References

[1] Reddy, J. N., Berry, J., 2012. Nonlinear theories of axisymmetric bending of functionally graded circular plates with modified couple stress. *Composite Structures*, 94(12), pp. 3664-3668.

[2] Reddy, J.N., Romanoff, J., Loya, J.A., 2016. Nonlinear finite element analysis of functionally graded circular plates with modified couple stress theory. *European Journal of Mechanics A/Solids*, 56, pp. 92-104.

[3] Dastjerdi, S., Jabbarzadeh, M., 2017. Non-linear bending analysis of multi-layer orthotropic annular/circular graphene sheets embedded in elastic matrix in thermal environment based on non-local elasticity theory. *Applied Mathematical Modelling*, 41, pp. 83-101.

[4] Dastjerdi, S., Jabbarzadeh, M., 2016. Non-Local Thermo-Elastic Buckling Analysis of Multi- Layer Annular/Circular Nano-Plates Based on First and Third Order Shear Deformation Theories Using DQ Method. *Journal of Solid Mechanics*, 8, pp. 859-874.

[5] Dastjerdi, S., Abbasi, M., Yazdanparast, L., 2017. A new modified higher-order shear deformation theory for nonlinear analysis of macro- and nano-annular sector plates using the extended Kantorovich method in conjunction with SAPM. *Acta Mechanica,* 228(10), pp. 3381-3401.

[6] Yang, B., Kitipornchai,S., Yang,Y.F., Yang, J., 2017. 3D thermo-mechanical bending solution of functionally graded graphene reinforced circular and annular plates. *Applied Mathematical Modelling,* 49, pp. 69-86.

[7] Reddy J.N., Berry J., 2012. Nonlinear theories of axisymmetric bending of functionally graded circular plates with modified couple stress, *Compos Struct*, 94(12), pp. 3664-3668.

[8] Reddy J.N., Kim J., 2012. A nonlinear modified couple stress-based third-order theory of functionally graded plates, *Compos Struct*, 94, pp. 1128-1143.

[9] Dastjerdi S., Jabbarzadeh M., 2016. Nonlinear bending analysis of bilayer orthotropic graphene sheets resting on Winkler-Pasternak elastic foundation based on Nonlocal Continuum Mechanics, *Compos Part B,* 87, pp. 161-175.

[10] Dastjerdi S., Jabbarzadeh M., Aliabadi S., 2016. Nonlinear static analysis of single layer annular/circular graphene sheets embedded in Winkler–Pasternak elastic matrix based on non-local theory of Eringen. *Ain Shams Eng. J.*, 7, pp. 873-884.

[11] Dastjerdi S., Lotfi M., Jabbarzadeh M., 2016. The effect of vacant defect on bending analysis of graphene sheets based on the Mindlin nonlocal elasticity theory. *Compos Part B*, 98, pp. 78-87.

[12] Dastjerdi S., Jabbarzadeh M., 2017. Non-linear bending analysis of multi-layer orthotropic annular/circular graphene sheets embedded in elastic matrix in thermal environment based on non-local elasticity theory. *App. Math. Model.*, 41, pp. 83-101.

[13] Dastjerdi S., Jabbarzadeh M., 2016. Nonlocal Bending Analysis of Bilayer Annular/Circular Nano Plates Based on First Order Shear Deformation Theory. *J. of Solid Mech*, 8, pp. 645-661.

[14] Dastjerdi S., Jabbarzadeh M., 2016. Non-Local Thermo-Elastic Buckling Analysis of Multi- Layer Annular/Circular Nano-Plates Based on First and Third Order Shear Deformation Theories Using DQ Method. *J. of Solid Mech.*, 8, pp. 859-874.

[15] Thai H.T., Choi D.H., 2013. Size-dependent functionally graded Kirchhoff and Midline plate models based on a modified couple stress theory. *Compos Struct*, 95, pp. 142-153.

[16] Thai H.T., Kim Se., 2013. A size-dependent functionally graded Reddy plate model based on a modified couple stress theory. *Compos Part B*, 50, pp. 1636-1645.

[17] Thai H.T., Vo T.P., 2013. A size-dependent functionally graded sinusoidal plate model based on a modified couple stress theory. *Compos Struct*, 96, pp. 376-383.

[18] Sahmani S., Ansari R., 2013. On the free vibration response of functionally graded higher-order shear deformable microplates based on the strain gradient elasticity theory. *Compos Struct*, 95, pp. 430-442.

[19] Daneshmehr A., Rajabpoor A., pourdavood M., 2014. Stability of size dependent functionally graded nanoplate based on nonlocal elasticity and higher order plate theories and different boundary conditions. *Int. J. Eng. Sci.*, 82, pp. 84-100.

[20] Tielking, J.T., 1979. Asymmetric bending of annular plated. *International Journal of Solid Structures,* 16, pp. 361-373.

[21] Pardoen, G.C., 1975. Asymmetric bending of circular plates using the finite element method. *Computers& Structures,* 5, pp. 197-202.

[22] Al Jarbouh, A., 2015. Mechanical Modelling for the Behavior of the Metallic Plate under the Effect of Bending Loads. *Energy Procedia*, 74, pp. 1119-32.

[23] Asadi Jafari, M.H., Zarastvand, M.R., Zhou, J., 2023. Doubly curved truss core composite shell system for broadband diffuse acoustic insulation. Journal, 30, pp. 17-18.

[24] Zarastvand, M.R., Ghassabi, M., Talebitooti, R., 2021. A Review Approach for Sound Propagation Prediction of Plate Constructions. *Archives of Computational Methods in Engineering*, 28, pp. 2817–2843.

[25] Zarastvand, M.R., Ghassabi, M., Talebitooti, R., 2021. Prediction of acoustic wave transmission features of the multilayered plate constructions: A review. *Journal of Sandwich Structures & Materials*, 24, 1.

[26] Zarastvand, M., Talebitooti, R., 2018. The effect of nature of porous material on diffuse field acoustic transmission of the sandwich aerospace composite doubly curved shell. *Aerospace Science and Technology*, 78, pp. 157-170.

[27] Timoshenko, S., Woinowsky-Krieger, S., 1959. *Theories of Plates and Shells*. New York, McGraw-Book Company.

[28] Reddy, J.N., Wang, C.M., Kitipornchai, S., 1999. Axisymmetric bending of functionally grade circular and annular plates. *European Journal of Mechanics A/Solids,* 18, pp. 185-99.

[29] Sahraee, S., Saidi, A.R., 2009. Axisymmetric bending analysis of thick functionally graded circular plates using fourth-order shear deformation theory. *European Journal of Mechanics A/Solids,* 28, pp. 974–984.